ELSEVIER

Contents lists available at ScienceDirect

Mechanics of Materials

journal homepage: www.elsevier.com/locate/mecmat



Research paper

Approximate analysis of necklace coalescence

M.E. Torki a,b, A.A. Benzerga b,c,*, J.-B. Leblond d

- ^a School of Engineering and Applied Science, University of Pennsylvania, Philadelphia, PA 19104, USA
- ^b Department of Aerospace Engineering, Texas A&M University, College Station, TX 77843, USA
- ^c Department of Materials Science and Engineering, Texas A&M University, College Station, TX 77843, USA
- d Sorbonne Universites, UPMC Univ Paris 06, CNRS, UMR 7190 Institut Jean Le Rond d'Alembert, F-75005, Paris, France

ARTICLE INFO

Keywords: Ductile fracture Porous plasticity Strain localization Void growth Delamination

ABSTRACT

Two recent models of void coalescence in columns are revisited to provide simpler, approximate expressions for the effective yield surface. Unlike the exact criteria, these are not upper-bound preserving but provide more flexibility in numerical implementation of the models. Both models correspond to limit analysis on the same geometry, namely a cylindrical void of finite height embedded in a cylindrical cell. One model employs a continuous velocity field, the other a discontinuous, yet kinematically admissible velocity field. The approximations are assessed by direct comparison to the exact criteria for several sets of the internal parameters.

1. Introduction

Void coalescence is the ultimate elementary stage of ductile failure. Internal necking (Thomason, 1968) and coalescence under combined tension and shear (Tvergaard, 1981) are the most common mechanisms. In many situations, voids link up along their main direction leading to columns of ruined material. This mechanism is called *necklace coalescence* or *void coalescence in columns*; see Pineau et al. (2016).

The modeling of void coalescence from first principles has remained elusive until recent years, e.g. Benzerga and Leblond (2014). In particular, void coalescence in columns has rarely been analyzed (Gologanu et al., 2001). Yet, its role in ductile delamination (a type of splitting fractures) (Bramfitt and Marder, 1977; Wang et al., 2022) is paramount, even if not yet fully recognized. Cell model analyses have often been restricted to conditions where this phenomenon is not observed. Under axisymmetric loading with a major lateral stress, Gologanu et al. (2001) have shown that the loss of load bearing capacity does not occur due to the elastic unloading that accompanies internal necking, rather to a more gradual softening due to the formation of columns of ruined material. More generally, other types of behavior may be observed in cell model analyses, e.g. Srivastava and Needleman (2013).

Very recently, the authors developed two micromechanical models of void coalescence in columns using limit analysis theory and tools from homogenization theory (Torki et al., 2023). In the first, they employed a discontinuous, but kinematically admissible velocity field, which led to a closed-form expression of the yield criterion of the effective porous medium in a state of coalescence. The regular part of the yield locus, however, involves transcendental functions. In the

second model, the authors used a continuous velocity field thereby producing a smooth yield surface, but that led to an implicit yield criterion.

In this technical note, we present an approximate analysis of the same two problems with the aim of producing more user-friendly expressions of the effective yield loci. The expressions are expected to be simpler for implementation in structural analysis codes. Both approximations are thoroughly assessed against the exact criteria developed by Torki et al. (2023) for various combinations of the internal parameters.

2. Problem statement

Effective yielding of a porous material is determined by the following variational principle:

$$\forall \mathbf{D}, \quad \mathbf{\Sigma} : \mathbf{D} \leq \mathbf{\Pi}(\mathbf{D}),$$

$$\Pi(\mathbf{D}) = \inf_{\mathbf{v} \in \mathcal{K}(\mathbf{D})} \left[\left\langle \sup_{\sigma^* \in \mathcal{C}} \sigma^*_{ij} \, d_{ij} \right\rangle + \frac{1}{\Omega} \int_{S} \sup_{\sigma^* \in \mathcal{C}} t_i^* \left[\left[v_i \right] \right] \, \mathrm{d}S \right] \tag{1}$$

where $\langle \cdot \rangle_{\Omega}$ stands for averaging over domain Ω , $\Sigma \equiv \langle \sigma \rangle$, $\mathbf{D} \equiv \langle \mathbf{d} \rangle$, $\llbracket \mathbf{v} \rrbracket$ is the velocity jump across an interface S, \mathbf{t}^* is the surface traction, and $\Pi(\mathbf{D})$ is the effective plastic dissipation. Also, $\mathcal{K}(\mathbf{D})$ denotes the set of kinematically admissible and incompressible velocity fields \mathbf{v} associated with \mathbf{D} and C is the convex of reversibility. The material is modeled as rigid–ideally plastic and obeying J_2 flow theory. If $\Pi(\mathbf{D})$

https://doi.org/10.1016/j.mechmat.2023.104603

^{*} Correspondence to: Texas A&M University, College Station, TX 77845-3141. E-mail address: benzerga@tamu.edu (A.A. Benzerga).

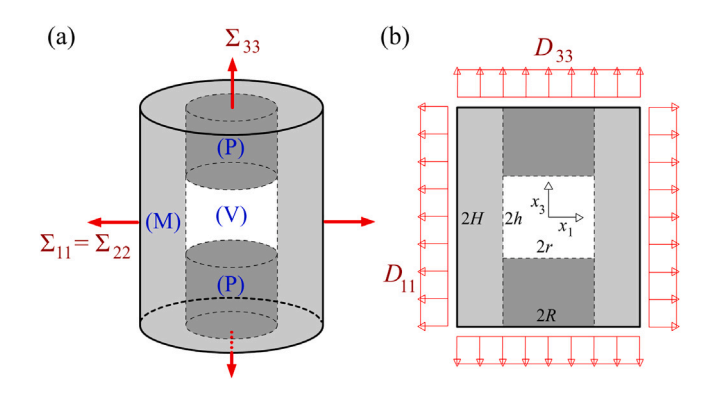


Fig. 1. (a) Cylindrical cell representing column coalescence under triaxial loading. (b) Meridian section of the cell, also showing the overall rate-of-deformation.

is differentiable then the effective yield surface is parametrically given by:

$$\Sigma = \frac{\partial \Pi}{\partial \mathbf{D}} \tag{2}$$

where Π now reduces to the first (volume) term in Eq. (1)₂; see Benzerga and Leblond (2010).

To treat void coalescence in columns, Torki et al. (2023) used (1) or Eq. (2) to carry out the limit analysis of an elementary cylindrical cell embedding a coaxial cylindrical void under axisymmetric loading, Fig. 1. They divided the cell in three subparts: the void (V), the matrix (M) exclusive of plugs, and the plugs (P). The cell geometry is entirely defined by three parameters out of the following:

$$f = \frac{\omega}{\Omega}, \quad \chi = \frac{r}{R}, \quad w = \frac{h}{r}, \quad \lambda = \frac{H}{R}, \quad c = \frac{h}{H}$$
 (3)

where ω , r and h denote the volume, radius and height of the void, R and H the cell's radius and height. Thus, f is the void volume fraction, χ the transverse ligament parameter, w the void aspect ratio, λ the cell aspect ratio, and c the axial ligament parameter.

During coalescence in columns, a finite strain concentration occurs in the plugs. Using strain compatibility and matrix incompressibility, one can relate the average rates of deformation in the matrix and porous regions to their macroscopic counterparts, leading to specific constraints on the velocity fields to be used in limit analysis. The simplest velocity field used by Torki et al. (2023) is given in cylindrical coordinates (ρ, θ, z) by:

$$v_{\rho}^{(M)} = \frac{R}{2} \left[D_{kk} \frac{R}{\rho} - D_{33} \frac{\rho}{R} \right], \quad v_{z}^{(M)} = D_{33} z \quad \text{in the matrix}$$
 (4)

$$v_{\rho}^{(P)} = \frac{1}{2} \left(\frac{D_{kk}}{\chi^2} - D_{33} \right) \rho, \qquad v_z^{(P)} = \frac{D_{kk}}{\chi^2} (H - z) + D_{33} z \qquad \text{in the plugs}$$
(5)

The field in Eq. (5) is discontinuous across the P-M interface with:

$$[v_z(z)]_{\rho=r} = \frac{D_{kk}}{\gamma^2} (H - z)$$
 (6)

Thus, Torki et al. (2023) introduced an alternative, continuous field given by:

$$\begin{cases} v_{\rho}^{(P)} = -\frac{\rho}{2} \left\{ D_{33} + \frac{D_{kk}}{\chi^2} \left[-2 + \left(\frac{\rho}{r} \right)^2 \right] \right\} \\ v_{z}^{(P)} = 2 \left[1 - \left(\frac{\rho}{r} \right)^2 \right] \frac{D_{kk}}{\chi^2} (H - z) + D_{33} z \end{cases}$$
 (7)

The dissipation function corresponding to the discontinuous velocity field $\{Eq. (4), Eq. (5)\}$ was calculated as:

$$\Pi = \Pi^{(M)} + \Pi^{(P)} + \Pi^{\text{surf}} \tag{8}$$

with

$$\Pi^{(M)} = \bar{\sigma} \frac{|D_{kk}|}{\sqrt{3}} \left[\sqrt{1 + \left(\frac{u}{\xi}\right)^2} - \sinh^{-1}\left(\frac{\xi}{u}\right) \right]_{u=2}^1, \qquad \xi = \frac{D_{kk}}{\sqrt{3}D_{33}}$$
(9)

$$\Pi^{(P)} = (1 - c)\bar{\sigma} \left| D_{kk} - \chi^2 D_{33} \right| \tag{10}$$

$$\Pi^{\text{surf}} = \frac{w(1-c)^2}{\sqrt{3}c}\bar{\sigma}|D_{kk}|\tag{11}$$

where w and c are defined in Eq. (3) and $\bar{\sigma}$ is the matrix yield strength. The function $\Pi^{(\mathrm{M})}(\mathbf{D})$ is differentiable. The term $|D_{kk}|$ appears therein only because of using the dimensionless parameter ξ . On the other hand, the functions $\Pi^{(\mathrm{P})}$ and Π^{surf} are not differentiable.

On the other hand, for the continuous velocity field {Eq. (4), Eq. (7)}, Torki et al. (2023) found that:

$$\Pi = \Pi^{(M)} + \Pi^{(P)} \tag{12}$$

with $\Pi^{(M)}$ still given by Eq. (9) and

$$\Pi^{(P)} = \bar{\sigma} |D_{33}| \chi^2 \int_c^1 \mathcal{I}(v) \, dv, \qquad \mathcal{I}(v) = \int_0^1 \sqrt{\mathcal{R}(u, v)} \, du$$
(13)

where (see Appendix)

$$\mathcal{R}(u,v) = \mathcal{U}_0 + 2\mathcal{U}_1(v)u + \mathcal{U}_2u^2 \tag{14}$$

$$\mathcal{U}_0 = (\bar{\xi} - 1)^2, \quad \mathcal{U}_1 = \bar{\xi} + \bar{\xi}^2 (\delta(v) - 1), \quad \mathcal{U}_2 = \frac{13}{12} \bar{\xi}^2$$
 (15)

$$\bar{\xi} = 2\sqrt{3} \frac{\xi}{v^2}, \quad \delta(v) = \frac{2}{3} \left(\frac{w(1-v)}{c}\right)^2$$
 (16)

Using Eqs. (8) and (12) in either (1) or Eq. (2), Torki et al. (2023) developed two yield criteria for coalescence in columns. They are both quite complex. Here, simpler forms are sought.

3. Approximate yield criteria

3.1. Using the discontinuous field

The dissipation term $\Pi^{(\mathrm{M})}$ in Eq. (8), which actually results from exact integration of:

$$\Pi^{(M)} = \bar{\sigma} |D_{33}| \int_{\gamma^2}^1 \sqrt{\left(\frac{\xi}{u}\right)^2 + 1} du$$
 (17)

is replaced with the approximate integral

$$H^{(M)} \approx \bar{\sigma} |D_{33}| (1 - \chi^2) \sqrt{\left(\frac{\xi}{1 - \chi^2} \int_{\chi^2}^1 \frac{du}{u}\right)^2 + 1}$$

$$= \bar{\sigma} |D_{33}| \sqrt{\left(\ln \frac{1}{\chi^2}\right)^2 \xi^2 + \left(1 - \chi^2\right)^2}$$
(18)

instead of the exact integral of Eq. (9). In going from Eq. (17) to Eq. (18) we have used

$$\left\langle \sqrt{f(\xi)^2 + C} \right\rangle \approx \sqrt{\langle f(\xi) \rangle^2 + C}$$
 (19)

for any positive function f and positive constant C. The above approximation becomes exact in two cases: (i) when the function f is constant, and (ii) when C is zero. But it loses the upper-bound character of the approach. The latter would be preserved if the mean of the square of f were used. This alternative approximation is still exact in special case (i) but not in (ii). Eq. $(18)_2$ leads to a relatively simpler yield criterion.

The dissipation function given by Eq. (8) is non-differentiable owing to the presence of absolute values in the expressions of Eq. (10) and Eq. (11) of $\Pi^{(P)}$ and Π^{surf} . This leads to singular parts on the yield locus, which must be analyzed with care. Obtaining a yield criterion using the velocity field defined by {Eq. (4), Eq. (5)} must then proceed

from inequality (1). The latter is rewritten for both pairs (D_{kk} , D_{33}) and ($-D_{kk}$, $-D_{33}$) so as to only consider non-negative values of D_{33} . The function $\Pi(D_{kk}, D_{33})$ being even one gets:

$$\forall D_{kk}, D_{33}, \quad D_{33} \ge 0$$

$$-\Pi(D_{kk}, D_{33}) \le \Sigma_{11} D_{kk} + (\Sigma_{33} - \Sigma_{11}) D_{33} \le \Pi(D_{kk}, D_{33})$$
(20)

Dividing all sides by D_{33} and using the fact that Π is positively homogeneous of degree 1, one gets:

$$\forall \xi \in \mathbb{R} \qquad -g(\xi) \le f(\xi) \le g(\xi) \tag{21}$$

where:

$$f(\xi) = \sqrt{3} \Sigma_{11} \xi + \Sigma_{33} - \Sigma_{11}$$

$$\frac{1}{\bar{\sigma}} g(\xi) = \frac{1}{\bar{\sigma}} \Pi(\sqrt{3}\xi, 1)$$

$$= \sqrt{\left(\ln \frac{1}{\chi^2}\right)^2 \xi^2 + \left(1 - \chi^2\right)^2} + (1 - c) \left|\sqrt{3}\xi - \chi^2\right| + w \frac{(1 - c)^2}{c} |\xi|$$
(22)

Let $Q(\xi)$ denote the first term in $g(\xi)/\bar{\sigma}$. Then,

$$\frac{1}{\bar{\sigma}}g'(\xi) = \left(\ln\frac{1}{\chi^2}\right)^2 \frac{\xi}{Q(\xi)} + \sqrt{3}(1-c)\operatorname{sgn}\left(\sqrt{3}\xi - \chi^2\right) + w\frac{(1-c)^2}{c}\operatorname{sgn}(\xi)$$

The curve $\zeta=f(\xi)$ is a straight line parameterized by Σ_{11} and Σ_{33} . On the other hand, the curves $\zeta=g(\xi)$ (sketched in Fig. 2) and $\zeta=-g(\xi)$ have the following characteristics:

- The curve $\zeta = g(\xi)$ is convex while the curve $\zeta = -g(\xi)$ is concave.
- The expression of $g(\xi)$ in Eq. (22) contains terms proportional to $|\sqrt{3}\xi \chi^2|$ and $|\xi|$. It follows that the curves $\zeta = g(\xi)$ and $\zeta = -g(\xi)$ have angular points at $\xi = 0$ and $\xi = \chi^2/\sqrt{3}$; except at these points the curves are smooth.
- Both curves admit straight asymptotes for $\xi \to \pm \infty$; in addition, the asymptote to the curve $\zeta = -g(\xi)$ for $\xi \to +\infty$ (resp. $\xi \to -\infty$) coincides with the asymptote to the curve $\zeta = g(\xi)$ for $\xi \to -\infty$ (resp. $\xi \to +\infty$).

A graphical method is then implemented to solve the inequalities in (21). In order for the pair $(\Sigma_{11}, \Sigma_{33})$ to lie on the yield locus, the straight line $\zeta = f(\xi)$ must meet one of the curves $\zeta = g(\xi)$, $\zeta = -g(\xi)$ at some point, *without crossing it*. Exploiting the point symmetry of the yield locus, we only consider half of it. This portion is determined when the straight line $\zeta = f(\xi)$ meets the curve $\zeta = g(\xi)$ without crossing it. This may occur in three cases:

1. The line $\zeta = f(\xi)$ meets the curve $\zeta = g(\xi)$ at $\xi = 0$ and lies between the two tangents to this curve at this point, Fig. 2a. The ordinate of the line at the origin is thus fixed, $f(0) = \Sigma_{33} - \Sigma_{11} = g(0)$. Its slope, on the other hand, may vary between bounds: namely, $g'(0^-) \leq f'(0) \leq g'(0^+)$. In other words, there is a straight (singular) portion on the yield locus, defined by:

$$\Sigma_{33} - \Sigma_{11} = \bar{\sigma}(1 - c\chi^2)$$
 for $\left| \frac{\Sigma_{11}}{\bar{\sigma}} + (1 - c) \right| \le \frac{w}{\sqrt{3}} \frac{(1 - c)^2}{c}$ (24)

since from Eq. (22) $g'(0^{\pm})/\bar{\sigma} = -\sqrt{3}(1-c) \pm w(1-c)^2/c$. Fig. 2b depicts the straight portion as two segments, plotted in the half plane $\Sigma_{\rm m} \geq 0$ for convenience.

2. The line $\zeta = f(\xi)$ meets the curve $\zeta = g(\xi)$ at $\xi = \chi^2/\sqrt{3}$ and lies between the two tangents to the curve at this point, Fig. 2c. Here, the ordinate is $f(\chi^2/\sqrt{3}) = \Sigma_{33} - (1 - \chi^2)\Sigma_{11}$ and the slope may vary between $g'(\chi^2/\sqrt{3})$ and $g'(\chi^2/\sqrt{3})$. In this case, the

vield condition is then:

$$\frac{1}{\bar{\sigma}}f\left(\frac{\chi^2}{\sqrt{3}}\right) = \frac{1}{\bar{\sigma}}g\left(\frac{\chi^2}{\sqrt{3}}\right) = \sqrt{\left(\ln\frac{1}{\chi^2}\right)^2\frac{\chi^4}{3} + \left(1 - \chi^2\right)^2} + \frac{\chi^2}{\sqrt{3}}w\frac{(1 - c)^2}{c}$$
(25)

subject to the condition $g'(\chi^2/\sqrt{3}^-) \le f'(\chi^2/\sqrt{3}) \le g'(\chi^2/\sqrt{3}^+)$ where:

$$\frac{1}{\bar{\sigma}}g'\left(\frac{\chi^2}{\sqrt{3}}^{\pm}\right) = B \pm C \quad \text{with}$$
 (26)

$$B = \left(\ln \frac{1}{\chi^2}\right)^2 \frac{\chi^2}{\sqrt{3}Q(\chi^2/\sqrt{3})} + w \frac{(1-c)^2}{c}$$

$$C = \sqrt{3}(1-c)$$
(27)

Thus, the second singular part of the yield locus is given by (see Fig. 2d):

$$(\Sigma_{33} - \Sigma_{11}) + \chi^2 \Sigma_{11} = A \quad \text{for} \quad \left| \frac{\Sigma_{11}}{\bar{\sigma}} - \frac{B}{\sqrt{3}} \right| \le \frac{C}{\sqrt{3}}$$
 (28)

where $A \equiv g(\chi^2/\sqrt{3})$, B and C are given by Eqs. (25) and (27).

3. The line $\zeta = f(\xi)$ is tangent to the curve $\zeta = g(\xi)$ at neither $\xi = 0$ nor $\xi = \chi^2/\sqrt{3}$, Fig. 3a. The ordinate of the line at the origin is then a smooth function of its slope; this means that the stress point lies on the regular part of the yield locus, which is curved, Fig. 3b.

The yield locus is now parametrically defined by Eq. (2), which on account of Eq. (8), is expressed as:

$$\Sigma_{11} = \frac{\partial \Pi}{\partial D_{kk}} = \frac{\partial \Pi^{(M)}}{\partial D_{kk}} + \frac{\partial \Pi^{(P)}}{\partial D_{kk}} + \frac{\partial \Pi^{\text{surf}}}{\partial D_{kk}}
\Sigma_{33} - \Sigma_{11} = \frac{\partial \Pi}{\partial D_{33}} = \frac{\partial \Pi^{(M)}}{\partial D_{33}} + \frac{\partial \Pi^{(P)}}{\partial D_{33}} + \frac{\partial \Pi^{\text{surf}}}{\partial D_{33}}$$
(29)

Define

$$\Sigma^{(M)} = \frac{\partial \Pi^{(M)}}{\partial \mathbf{D}} \tag{30}$$

with $\Pi^{(\mathrm{M})}$ defined by Eq. (18). Then, taking axial symmetry into account,

$$\Sigma_{11}^{(M)} = \bar{\sigma}a^2 \frac{D_{kk}}{\sqrt{a^2 D_{kk}^2 + b^2 D_{33}^2}}
\Sigma_{33}^{(M)} - \Sigma_{11}^{(M)} = \bar{\sigma}b^2 \frac{D_{33}}{\sqrt{a^2 D_{kk}^2 + b^2 D_{33}^2}}$$
(31)

where $a = \sqrt{3} \ln(1/\chi^2)$ and $b = 1 - \chi^2$. Eliminating ξ leads to:

$$\left[\frac{\Sigma_{33}^{(M)} - \Sigma_{11}^{(M)}}{(1 - \chi^2)\bar{\sigma}}\right]^2 + 3 \left[\frac{\Sigma_{11}^{(M)}}{\ln\left(\frac{1}{\chi^2}\right)\bar{\sigma}}\right]^2 = 1$$
 (32)

Using the expressions of $\Pi^{(P)}$ and Π^{surf} , Eqs. (10) and (11), the remaining four terms in Eq. (29) are:

$$\begin{split} &\frac{\partial \boldsymbol{\varPi}^{(\mathrm{P})}}{\partial \boldsymbol{D}_{kk}} = &(1-c)\bar{\sigma}\mathrm{sgn}\left(\boldsymbol{D}_{kk} - \chi^2\boldsymbol{D}_{33}\right), \quad \frac{\partial \boldsymbol{\varPi}^{\mathrm{surf}}}{\partial \boldsymbol{D}_{kk}} = \frac{w}{\sqrt{3}}\frac{(1-c)^2}{c}\bar{\sigma}\mathrm{sgn}\left(\boldsymbol{D}_{kk}\right) \\ &\frac{\partial \boldsymbol{\varPi}^{(\mathrm{P})}}{\partial \boldsymbol{D}_{33}} = &-(1-c)\chi^2\bar{\sigma}\mathrm{sgn}\left(\boldsymbol{D}_{kk} - \chi^2\boldsymbol{D}_{33}\right), \quad \frac{\partial \boldsymbol{\varPi}^{\mathrm{surf}}}{\partial \boldsymbol{D}_{33}} = 0 \end{split}$$

(33)

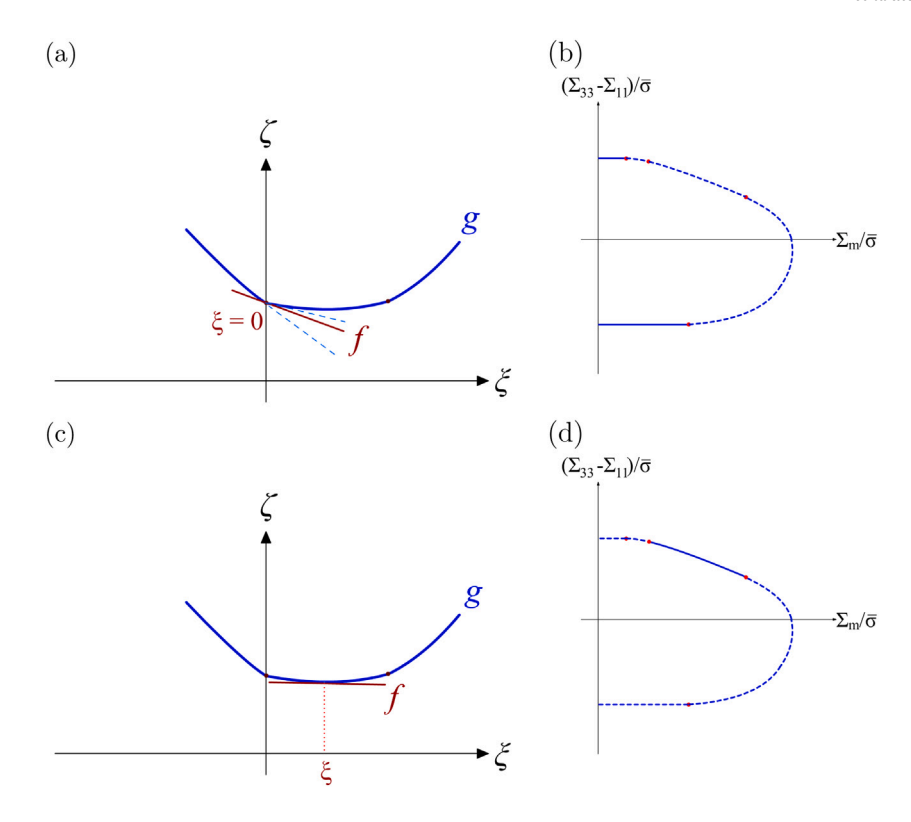


Fig. 2. Graphical solution to Eq. (21). (a) Case of $\xi = 0$ leading to first type of singular parts on yield locus depicted in (b). (c) Case of $\xi = \chi^2/\sqrt{3}$ leading to second type of singular parts on yield locus depicted in (d).

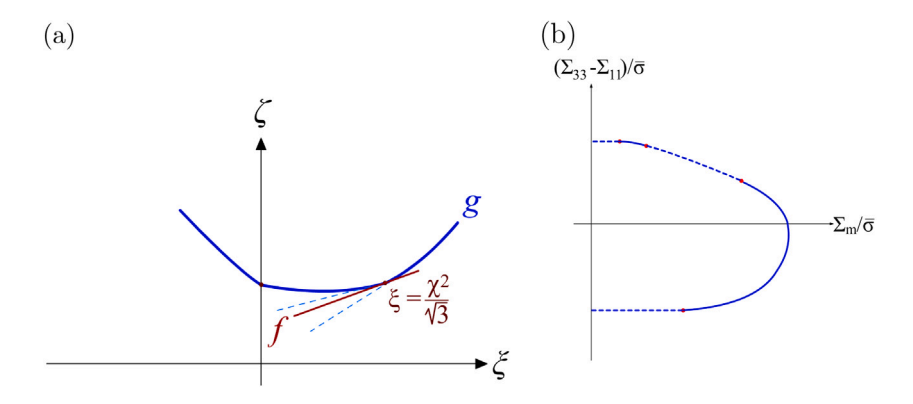


Fig. 3. Graphical solution to Eq. (21). (a) Case of $\xi \neq 0, \xi \neq \chi^2/\sqrt{3}$ leading to regular, curved part on yield locus depicted in (b).

Then substituting for $\Sigma_{11}^{(\mathrm{M})}$ and $\Sigma_{33}^{(\mathrm{M})}$ their expressions given by Eq. (29) into Eq. (32), with due account for Eq. (33), delivers the final expression for the regular portion of the yield locus:

$$\begin{split} & \left[\frac{\Sigma_{33} - \Sigma_{11}}{(1 - \chi^2)\bar{\sigma}} + \epsilon_1 \frac{(1 - c)\chi^2}{1 - \chi^2} \right]^2 \\ & + \frac{3}{4(\ln \chi)^2} \left[\frac{\Sigma_{11}}{\bar{\sigma}} - \epsilon_1 (1 - c) - \epsilon_2 \frac{w}{\sqrt{3}} \frac{(1 - c)^2}{c} \right]^2 = 1 \end{split}$$
(34)

with $\epsilon_1 = \text{sgn} \left(D_{kk} - \chi^2 D_{33}\right)$ and $\epsilon_2 = \text{sgn} \left(D_{kk}\right)$ giving rise to four distinct regular portions of the yield locus, two of which are represented in Fig. 3. On the other hand, Eqs. (24) and (28) only determine two segments of the singular parts. The other two are obtained by point symmetry of the yield locus.

3.1.1. Synopsis

In summary, the yield locus is defined by the following:

$$\Sigma_{33} - \Sigma_{11} = \pm \bar{\sigma} (1 - c\chi^{2}) \quad \text{for} \quad \left| \frac{\Sigma_{11}}{\bar{\sigma}} \pm (1 - c) \right| \leq \frac{w}{\sqrt{3}} \frac{(1 - c)^{2}}{c} \\
(\Sigma_{33} - \Sigma_{11}) + \chi^{2} \Sigma_{11} = \pm A \quad \text{for} \quad \left| \frac{\Sigma_{11}}{\bar{\sigma}} \mp \frac{B}{\sqrt{3}} \right| \leq 1 - c \\
\left[\frac{\Sigma_{33} - \Sigma_{11}}{(1 - \chi^{2})\bar{\sigma}} + \epsilon_{1} \frac{(1 - c)\chi^{2}}{1 - \chi^{2}} \right]^{2} \\
+ \frac{3}{4(\ln \chi)^{2}} \left[\frac{\Sigma_{11}}{\bar{\sigma}} - \epsilon_{1} (1 - c) - \epsilon_{2} \frac{w}{\sqrt{3}} \frac{(1 - c)^{2}}{c} \right]^{2} = 1$$
(35)

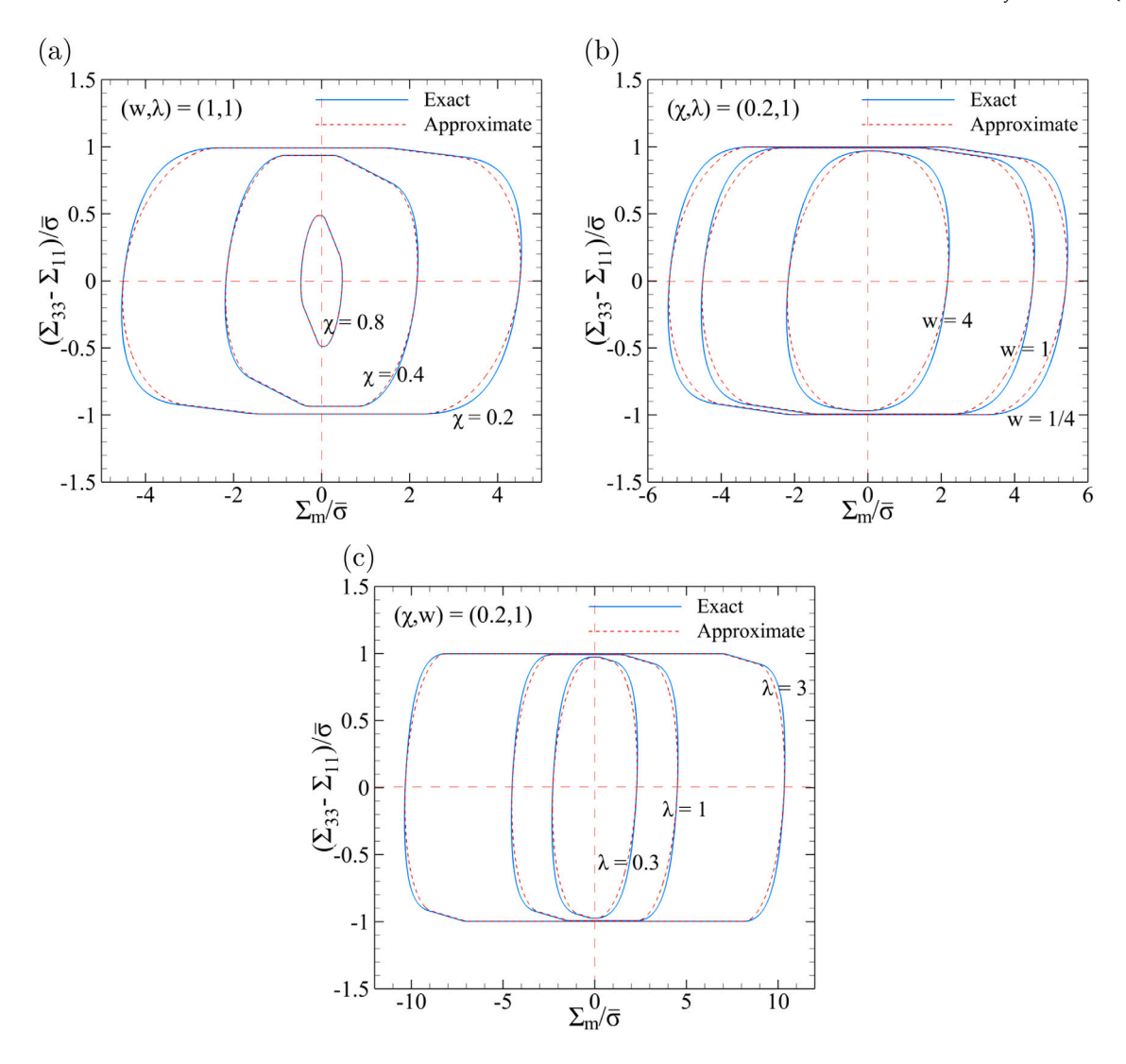


Fig. 4. Comparison between minimum-continuity yield surfaces based on exact and approximate integrations: (a) for fixed (w, λ) and various ligament parameters χ , (b) for fixed (χ, λ) and various void aspect ratios w, (c) for fixed (χ, w) and various cell aspect ratios λ .

where A and B in Eq. $(35)_2$ are functions of the internal parameters given by:

$$\frac{A}{\bar{\sigma}} = Q\left(\frac{\chi^2}{\sqrt{3}}\right) + \frac{\chi^2}{\sqrt{3}} w \frac{(1-c)^2}{c}$$

$$B = \left(\ln\frac{1}{\chi^2}\right)^2 \frac{\chi^2}{\sqrt{3}Q(\chi^2/\sqrt{3})} + w \frac{(1-c)^2}{c}$$
(36)

 $\epsilon_1=\mathrm{sgn}\left(D_{kk}-\chi^2D_{33}\right)$, $\epsilon_2=\mathrm{sgn}\left(D_{kk}\right)$, and in Eq. (36) the function $Q(\xi)$ is defined by:

$$Q(\xi) = \sqrt{\left(\ln\frac{1}{\chi^2}\right)^2 \xi^2 + \left(1 - \chi^2\right)^2}$$
 (37)

Fig. 4 shows comparisons between the surfaces corresponding to the exact and approximate forms of the yield function for various values of the void aspect ratio, ligament parameter, and cell aspect ratio. Although the approximate criterion loses the upper-bound character, it stays close to the rigorous upper-bound criterion.

3.2. Using the continuous field

To obtain a closed-form solution in this case, the following approximation is adopted in Eq. (13):

$$\Pi^{(P)} = \bar{\sigma} |D_{33}| \chi^2 \int_c^1 \mathcal{I}(v) dv \approx \bar{\sigma} |D_{33}| \chi^2 (1 - c) \bar{\mathcal{I}}$$
(38)

where \bar{I} is given by:

$$\bar{I} = \frac{1}{2} \left[(u + B) \sqrt{\bar{R}(u)} + \mathcal{P} \ln |\mathcal{L}(u)| \right]_{u=0}^{1}$$
(39)

for $\Delta = \mathcal{U}_0 \mathcal{U}_2 - \bar{\mathcal{U}}_1^2 > 0$ with

$$B = \frac{\bar{U}_{1}}{U_{2}} = \frac{12}{13} \left(\frac{1}{\bar{\xi}} + \bar{\delta} - 1 \right)$$

$$P = \frac{U_{0} - \frac{\bar{U}_{1}^{2}}{U_{2}}}{\sqrt{U_{2}}} = \sqrt{\frac{12}{13}} \frac{1}{|\bar{\xi}|} \left[(\bar{\xi} - 1)^{2} - \frac{12}{13} \left(1 + \bar{\xi}(\bar{\delta} - 1) \right)^{2} \right]$$

$$\mathcal{L} = \sqrt{V_{2}\bar{R}(u)} + V_{2}u + \bar{U}_{1}$$
(40)

The above results are formally identical to those corresponding to exact integration of Eq. (38)₁ following Gradshtein and Ryzhik (1971)

but with $\bar{\delta}$, \bar{U}_1 and $\bar{R}(u)$ appearing instead of $\delta(v)$, $V_1(v)$ and R(u,v) with:

$$\bar{\delta} \equiv \langle \sqrt{\delta} \rangle = \sqrt{\frac{2}{3}} \frac{w}{c} \left(\frac{1}{1-c} \int_{c}^{1} v \, dv \right) = \frac{w}{c} \frac{1+c}{\sqrt{6}}$$

the averaging being carried out over v in the interval [c, 1], and

$$\bar{U}_1 = \bar{\xi} + \bar{\xi}^2 \left[\langle \sqrt{\delta} \rangle^2 - 1 \right] = \bar{\xi} + \bar{\xi}^2 \left[\frac{1}{6} \left(\frac{w(1+c)}{c} \right)^2 - 1 \right] \tag{41}$$

while $\bar{R}(u)$ is given by Eq. (14) with $V_1(v)$ replaced by \bar{U}_1 . The case $\Delta < 0$ is rare and is considered in the same way as in Torki et al. (2023).

In this case, the yield surface is parametrically defined using Eq. (2). Based on Eq. (12) one may posit:

$$\Sigma = \Sigma^{(M)} + \Sigma^{(P)}$$
 with $\Sigma^{(M)} = \frac{\partial \Pi^{(M)}}{\partial \mathbf{D}}$ and $\Sigma^{(P)} = \frac{\partial \Pi^{(P)}}{\partial \mathbf{D}}$ (42)

where $\Pi^{(M)}$ is given by Eq. (9) and $\Pi^{(P)}$ by Eq. (38)₂. The dissipation $\Pi(\mathbf{D})$ is positively homogeneous of degree 1; hence its derivative with respect to \mathbf{D} is homogeneous of degree 0. Therefore, in Eq. (42) the stresses depend on the components of \mathbf{D} only through their ratios.

Taking the axial symmetry into account, the first term in Eq. (42)₁ is specified through:

$$\frac{\Sigma_{11}^{(M)}}{\bar{\sigma}} \operatorname{sgn}(D_{kk}) = \frac{1}{\sqrt{3}} \left(\sinh^{-1} |\xi| - \sinh^{-1} \frac{|\xi|}{\chi^2} \right)
\frac{\Sigma_{33}^{(M)} - \Sigma_{11}^{(M)}}{\bar{\sigma}} \operatorname{sgn}(D_{kk}) = \sqrt{1 + \xi^2} - \sqrt{\xi^2 + \chi^4}$$
(43)

where ξ is the strain rate ratio introduced in Eq. (9)₂. Note that the $\Pi^{(M)}$ term could also be approximated as it was treated in the "discontinuous" model. This would lead to an additional loss of accuracy.

To obtain the second term in Eq. $(42)_1$, note that \bar{I} in Eq. (39), depends on **D** through the ratio $\bar{\xi}$ as per Eqs. (14), (16) and (40). Thus,

$$\begin{split} & \Sigma_{11}^{(P)} = \frac{1}{2} \frac{\partial \Pi^{(P)}}{\partial D_{11}} = \frac{1}{2} \bar{\sigma} |D_{33}| \chi^2 (1-c) \frac{2}{\chi^2} \frac{2}{D_{33}} \frac{\partial \bar{I}}{\partial \bar{\xi}} \\ & \Sigma_{33}^{(P)} = \frac{\partial \Pi^{(P)}}{\partial D_{23}} = \bar{\sigma} \text{sgn} \left(D_{33}\right) \chi^2 (1-c) \bar{I} + \bar{\sigma} |D_{33}| \chi^2 (1-c) \frac{\partial \bar{I}}{\partial \bar{\xi}} \frac{\partial \bar{\xi}}{\partial D_{23}} \end{split} \tag{44}$$

where the factor 1/2 in the first equation accounts for the special axisymmetric loading considered throughout. Straight from Eq. (39) one gets:

$$\frac{\partial \bar{\mathcal{I}}}{\partial \bar{\mathcal{E}}} = \frac{1}{2} \left[\mathcal{B}' \sqrt{\bar{\mathcal{R}}} + (u + \mathcal{B}) \mathcal{R}^* + \mathcal{P}' \ln |\mathcal{L}| + \mathcal{P} \frac{\mathcal{L}'}{\mathcal{L}} \right]_{u=0}^{1}$$
(45)

where, with reference to the definitions in Eq. (40) and $\bar{\xi}$ from Eq. (16):

$$B' = \frac{\partial B}{\partial \bar{\xi}} = \frac{-12}{13\bar{\xi}^2}$$

$$P' = \frac{\partial P}{\partial \bar{\xi}} = \frac{\sqrt{12}}{13^{3/2}} \operatorname{sgn}(\bar{\xi}) \left[-2(\bar{\delta} - 1)^2 + 3 - \frac{1}{\bar{\xi}^2} \right]$$

$$\mathcal{R}^* = \frac{1}{2\sqrt{\bar{R}}} \frac{\partial \bar{R}}{\partial \bar{\xi}} = \frac{\frac{13}{12} \bar{\xi} u^2 + [1 + 2(\bar{\delta} - 1)\bar{\xi}] u + (\bar{\xi} - 1)}{\sqrt{\frac{13}{12} \bar{\xi}^2 u^2 + 2\bar{\xi}} [1 + (\bar{\delta} - 1)\bar{\xi}] u + (\bar{\xi} - 1)^2}$$

$$\mathcal{L}' = \frac{\partial \mathcal{L}}{\partial \bar{\xi}} = \sqrt{\frac{13}{12}} \left| \bar{\xi} \right| \mathcal{R}^* + \frac{13}{6} \bar{\xi} u + [1 + 2(\bar{\delta} - 1)\bar{\xi}]$$
(46)

After simplifying and rearranging, one finally has:

$$\frac{\Sigma_{11}^{(P)}}{\bar{\sigma}}\operatorname{sgn}\left(D_{33}\right) = 2(1-c)\frac{\partial\bar{I}}{\partial\bar{\xi}}$$

$$\frac{\Sigma_{33}^{(P)} - \Sigma_{11}^{(P)}}{\bar{\sigma}}\operatorname{sgn}\left(D_{33}\right) = \chi^{2}(1-c)\bar{I} - \chi^{2}\bar{\xi}(1-c)\frac{\partial\bar{I}}{\partial\bar{\xi}}$$
(47)

In summary, if the approximation in Eq. $(38)_2$ is used for the dissipation in the plugs, then a closed-form expression of the yield

surface is parametrically obtained as:

$$\begin{split} \frac{\Sigma_{11}}{\bar{\sigma}} &= \operatorname{sgn}\left(D_{kk}\right) \frac{1}{\sqrt{3}} \left(\sinh^{-1} |\xi| - \sinh^{-1} \frac{|\xi|}{\chi^2} \right) + 2 \operatorname{sgn}\left(D_{33}\right) (1 - c) \frac{\partial \bar{I}}{\partial \bar{\xi}} \\ \frac{\Sigma_{33} - \Sigma_{11}}{\bar{\sigma}} &= \operatorname{sgn}\left(D_{kk}\right) \left(\sqrt{1 + \xi^2} - \sqrt{\xi^2 + \chi^4}\right) \\ &+ \operatorname{sgn}\left(D_{33}\right) (1 - c) \chi^2 \left[\bar{I} - \bar{\xi} \frac{\partial \bar{I}}{\partial \bar{\xi}} \right] \end{split} \tag{48}$$

Alternatively, the integral in Eq. $(38)_1$ can be evaluated numerically. The corresponding yield surface is compared in Fig. 5 with that obtained using the approximation of Eq. $(38)_2$ leading to the criterion of Eq. (48). All surfaces have point symmetry with respect to the origin, but the useful part for potential coalescence in columns is expected to lie in the lower-right quadrant $(\Sigma_{33} - \Sigma_{11} < 0, \Sigma_m > 0)$, except for elongated voids (large values of w) or flat cells (small values of λ). While the employed approximation is not upper-bound preserving it provides a good estimate of the exact yield criterion.

We emphasize that the term "exact" in this paper signifies exact integration of the dissipation function. The true yield surface is not known analytically, but can be evaluated using numerical limit analysis. This was done in Torki et al. (2023) using a finite element method. Furthermore, the true yield surface is actually hybrid, in that parts of it may correspond to coalescence in columns while other parts would correspond to void growth and void coalescence in layers, as treated for example by Morin et al. (2016); see Torki et al. (2023) and references therein for more details.

4. Conclusion

Approximate yield criteria were obtained for a porous material in a state of void coalescence in columns. In the case of a discontinuous velocity field, the yield locus consists of straight singular parts and regular curved parts. It is the expression of the latter that was simplified in comparison with the reference exact expressions of Torki et al. (2023). In the case of a continuous velocity field, a closed-form expression in parametric form was obtained, unlike the expression of Torki et al. (2023), which was obtained using exact numerical integration. In both cases, the upper bound character of the yield locus is lost. However, detailed comparisons between approximate and exact criteria show that the approximate forms may be used in structural codes with no loss of accuracy over a wide range of values of the internal parameters. Circumstances under which coalescence in columns is favored include cases with elongated voids that are closely packed along their main axis, in keeping with experimental observations.

CRediT authorship contribution statement

M.E. Torki: Designed the research, Developed the analytical models and prepared all figures, Contributed to the analysis of the results and to writing the paper. A.A. Benzerga: Designed the research, Contributed to the analysis of the results and to writing the paper. J.-B. Leblond: Designed the research, Contributed to the analysis of the results and to writing the paper.

Declaration of competing interest

The authors declare that they have no known competing financial interests or personal relationships that could have appeared to influence the work reported in this paper.

Data availability

Data will be made available on request.

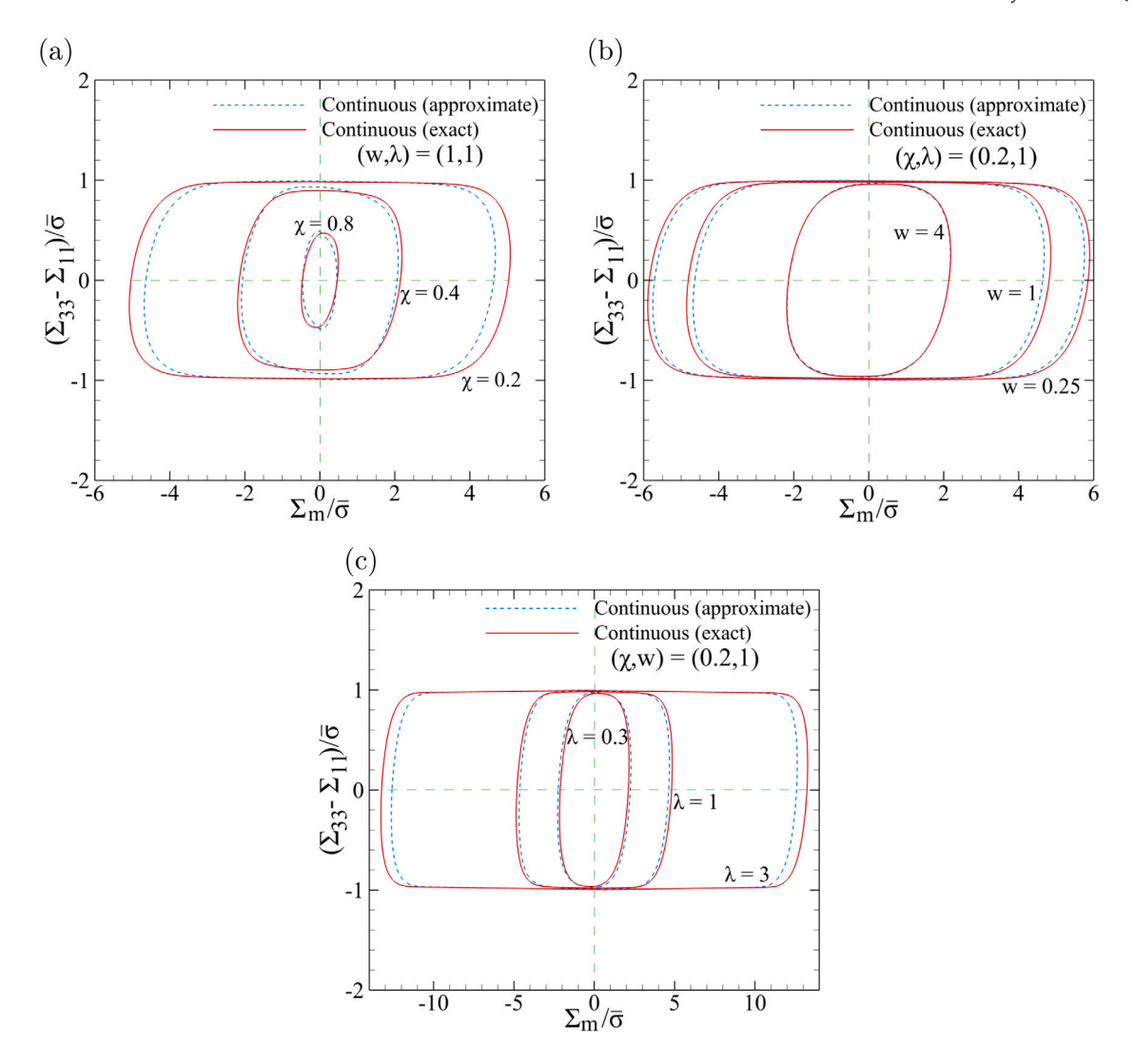


Fig. 5. Comparison between the exact and approximate yield surfaces obtained using a continuous velocity field (a) for fixed (w, λ) and various ligament parameters χ , (b) for fixed (χ, λ) and various void aspect ratios w, (c) for fixed (χ, w) and various cell aspect ratios λ .

Acknowledgments

This work was initiated with support from the National Science Foundation, United States under Grant Number CMMI-1405226. AAB acknowledges support from the National Science Foundation, United States (Grant Number CMMI-1932975).

Appendix. Derivation of Eq. (14)

A continuous velocity field is sought with an axial component given in separable form as:

$$v_z^{(P)}(\rho, z) = D_{33}z + f_0(z) + f_1(z)\rho^2$$
(A.1)

where functions $f_0(z)$ and $f_1(z)$ are determined so as to ensure continuity at the plug–matrix interface ($\rho=r$). On account of Eq. (4), this entails

$$\begin{split} v_z^{(\mathrm{P})}(r,z) &= v_z^{(\mathrm{M})}(z) = D_{33}z \quad \Rightarrow \quad f_0(z) + f_1(z)r^2 = 0 \\ v_\rho^{(\mathrm{P})}(r,z) &= v_\rho^{(\mathrm{M})}(r) = \left(\frac{D_{kk}}{\gamma^2} - D_{33}\right)\frac{r}{2} \end{split} \tag{A.2}$$

Incompressibility leads to the following relationship between the two components:

$$\operatorname{div} \mathbf{v}^{(P)} = \frac{1}{\rho} \frac{\partial (\rho v_{\rho}^{(P)})}{\partial \rho} + v_{z,z}^{(P)} = 0 \tag{A.3}$$

Combining Eqs. (A.1) and (A.3) delivers, after integration, the following expression for the radial component:

$$v_{\rho}^{(P)}(\rho, z) = -\left(D_{33} + f_0'(z)\right) \frac{\rho}{2} - f_1'(z) \frac{\rho^3}{4} \tag{A.4}$$

Its continuity across the plug–matrix interface, Eq. $(A.2)_2$, introduces a new relation between the derivatives of the two unknown functions f_0 and f_1 :

$$f_0'(z) + \frac{r^2}{2}f_1'(z) = -\frac{D_{kk}}{r^2} \tag{A.5}$$

Combining the above equation with Eq. $(A.2)_1$ gives after integration:

$$f_0(z) = -2\frac{D_{kk}}{\chi^2}z + g_0$$

$$f_1(z) = \frac{2}{r^2}\frac{D_{kk}}{\chi^2}z + g_1$$
(A.6)

where g_0 and g_1 are constants determined from strain-rate compatibility on the top surface, i.e. from the condition:

$$v_{z}^{(P)}(\rho, H) = D_{33}H, \quad \forall 0 \le \rho \le r$$
 (A.7)

which requires that $f_0(H) = f_1(H) = 0$. It follows that

$$f_0(z) = 2\frac{D_{kk}}{r^2}(H-z), \qquad f_1(z) = \frac{-f_0(z)}{r^2}$$
 (A.8)

Substituting the above results in Eqs. (A.1) and (A.4) leads to the continuous velocity field of Eq. (7).

Accordingly, obtain the rate of deformation components as:

$$\begin{split} d_{\rho\rho}^{(\mathrm{P})} &= v_{\rho,\rho}^{(\mathrm{P})} = \alpha_0 + \alpha_1 \rho^2 \\ d_{\theta\theta}^{(\mathrm{P})} &= \frac{v_{\rho}^{(\mathrm{P})}}{\rho} = \alpha_0 + \frac{1}{3}\alpha_1 \rho^2 \\ d_{zz}^{(\mathrm{P})} &= v_{z,z}^{(\mathrm{P})} = -2\alpha_0 - \frac{4}{3}\alpha_1 \rho^2 \\ d_{\rho z}^{(\mathrm{P})} &= d_{z\rho}^{(\mathrm{P})} = \frac{1}{2}v_{z,\rho}^{(\mathrm{P})} = \frac{4}{3}\alpha_1 \rho (H-z) \end{split} \tag{A.9}$$

where

$$\alpha_0 = -\frac{1}{2}D_{33} + \frac{1}{\chi^2}D_{kk}$$

$$\alpha_1 = -\frac{3}{2\chi^2}\frac{D_{kk}}{r^2}$$
(A.10)

The equivalent strain rate is then calculated as

$$d_{\text{eq}}^{(P)} \equiv \sqrt{\frac{2}{3}} \mathbf{d}^{(P)} : \mathbf{d}^{(P)} = \sqrt{\frac{2}{3} \left[\frac{26}{9} \alpha_1^2 \rho^4 + 8\alpha_0 \alpha_1 \rho^2 + \frac{32}{9} \alpha_1^2 (H - z)^2 \rho^2 + 6\alpha_0^2 \right]}$$
(A.11)

In terms of D_{kk} and D_{33} :

$$\begin{split} d_{\text{eq}}^{2(\text{P})} &= \frac{13}{3} \frac{D_{kk}^2}{\chi^4} \left(\frac{\rho}{r}\right)^4 + 4 \frac{D_{33} D_{kk}}{\chi^2} \left(\frac{\rho}{r}\right)^2 - 8 \frac{D_{kk}^2}{\chi^4} \left(\frac{\rho}{r}\right)^2 \\ &+ \frac{16}{3} \frac{D_{kk}^2}{\chi^4} \frac{H^2}{r^2} \left(1 - \frac{z}{H}\right)^2 \left(\frac{\rho}{r}\right)^2 + \\ D_{33}^2 + 4 \frac{D_{kk}^2}{\chi^4} - 4 \frac{D_{33} D_{kk}}{\chi^2} \end{split} \tag{A.12}$$

which may be put in the form:

$$d_{aa}^{(P)} = \sqrt{R} |D_{33}|, \qquad R = \mathcal{U}_0 + 2\mathcal{U}_1 u + \mathcal{U}_2 u^2 \tag{A.13}$$

the latter being Eq. (14) after operating the change of variable: $u = \rho^2/r^2$ and v = z/H and using the reduced variable $\bar{\xi}$ of Eq. (16) and the relation H/r = w/c.

References

Benzerga, A.A., Leblond, J.B., 2010. Ductile fracture by void growth to coalescence. Adv. Appl. Mech. 44, 169–305.

Benzerga, A.A., Leblond, J.B., 2014. Effective yield criterion accounting for microvoid coalescence. J. Appl. Mech. 81, 031009.

Bramfitt, B.L., Marder, A.R., 1977. A study of the delamination behavior of a very low-carbon steel. Metall. Trans. A 8, 1263–1273.

Gologanu, M., Leblond, J.B., Perrin, G., Devaux, J., 2001. Theoretical models for void coalescence in porous ductile solids – II: Coalescence in "columns". Int. J. Solids Struct. 38, 5595–5604.

Gradshtein, I.S., Ryzhik, I.M., 1971. Tables of integrals, sums, series and products.

Morin, L., Leblond, J., Benzerga, A.A., Kondo, D., 2016. A unified criterion for the growth and coalescence of microvoids. J. Mech. Phys. Solids 97, 19–36.

Pineau, A., Benzerga, A.A., Pardoen, T., 2016. Failure of metals I. Brittle and ductile fracture. Acta Mater. 107, 424–483.

Srivastava, A., Needleman, A., 2013. Void growth versus void collapse in a creeping single crystal. J. Mech. Phys. Solids 61, 1169–1184.

Thomason, P.F., 1968. A theory for ductile fracture by internal necking of cavities. J. Inst. Met. 96 (360).

Torki, M.E., Medrano, F.M., Benzerga, A.A., Leblond, J.B., 2023. A model of void coalescence in columns. J. Mech. Phys. Solids 171, 105134.

Tvergaard, V., 1981. Influence of voids on shear band instabilities under plane strain conditions. Int. J. Fract. 17, 389–407.

Wang, H., Tian, Y., Ye, Q., Wang, Q., Wang, Z., Wang, G., 2022. Effect of delamination on ductile fracture during the impact test in ultra-heavy steel. J. Mater. Eng. Perform. 31, 7843–7855.